A theoretical framework to analyse the behaviour of polymer geosynthetic reinforcement in temperature-accelerated creep tests

W. Kongkitkul[1] and F. Tatsuoka[2]

[1]*Postdoctoral Fellow, Department of Civil Engineering, Tokyo University of Science, 2641 Yamazaki, Noda, Chiba, 278-8510, Japan, Telephone: +81 4 7124 1501 (ext. 4074), Telefax: +81 4 7123 9766, E-mail: warat@rs.noda.tus.ac.jp*
[2]*Professor, Department of Civil Engineering, Tokyo University of Science, 2641 Yamazaki, Noda, Chiba, 278-8510, Japan, Telephone: +81 4 7122 9819, Telefax: +81 4 7123 9766, E-mail: tatsuoka@rs.noda.tus.ac.jp*

Received 8 May 2006, revised 6 October 2006, accepted 12 November 2006

ABSTRACT: A non-linear three-component model has been developed that can predict the strength and deformation of polymer geosynthetic reinforcement when subjected to arbitrary histories of strain, strain rate and temperature as encountered in the laboratory and in the field. An existing model framework assuming the elasto-viscoplastic property of material was modified to account for the effects of changes in ambient temperature on the load–strain relation. Tensile load–strain–time relations for typical geosynthetic reinforcement properties were obtained by direct simulations of long-term sustained loading (SL) tests at a fixed temperature as well as simulations of monotonic loading and sustained loading at different elevated temperatures in time–temperature superposition (TTS) and stepped isothermal method (SIM) tests. The procedures to obtain the master creep strain and modulus curves from the results of these three types of numerical analysis are presented and compared. Creep rupture curves constructed from the master curves obtained by direct simulations of long-term SL tests as well as the numerical TTS and SIM tests are compared. The creep rupture curves obtained by the three methods are similar for shorter creep rupture times, but they become different with an increase in the creep rupture time. The reasons for the difference are discussed. It is argued that the theoretical framework of the model is relevant and useful for analysing and interpreting results from TTS and SIM tests in a consistent manner.

KEYWORDS: Geosynthetics, Reinforcement, Creep, Time–temperature superposition, Stepped isothermal method, Non-linear three-component model, Numerical simulation

REFERENCE: Kongkitkul, W. & Tatsuoka, F. (2007). A theoretical framework to analyse the behaviour of polymer geosynthetic reinforcement in temperature-accelerated creep tests. *Geosynthetics International*, **14**, No. 1, 23–38

1. INTRODUCTION

In recent decades, a limited number of long-term creep rupture tests on polymer geosynthetic reinforcement have been performed to determine the so-called 'stress-rupture curves', as schematically illustrated in Figure 1. This type of test is highly time-consuming, and it is nearly impossible to perform tests of this type for a period of the usual design life of, say, 50 years. When polymeric material is subjected to elevated temperatures, its creep strain rate is accelerated, with a short time to rupture in creep tests (e.g. Ferry 1980), and the stiffness during monotonic loading (ML) at constant strain rate decreases (e.g. Zornberg & Kavazanjian 2002). In the time–temperature superposition (TTS) technique (e.g. Thornton *et al.* 1998), at a given constant tensile load, V, a set of creep tests are performed until rupture at a set of constant but different ambient temperatures, T. Then the so-called 'master curve', which is equivalent to the creep strain–log(time) relation from a long-term conventional creep test at a given tensile load V, is obtained by superimposing the creep strain–log(time) relations obtained at different ambient temperatures, T (as explained later in this paper). Subsequently, the stress-rupture curve (Figure 1) of a given type of geosynthetic reinforcement is obtained from master curves for different tensile loads, V.

The TTS technique needs multiple, highly replicated specimens to obtain a single reliable master curve. Furthermore, Thornton *et al.* (1998) reported that, even when the technique is performed at the same temperature, the inevitable variation in the load–strain curves from

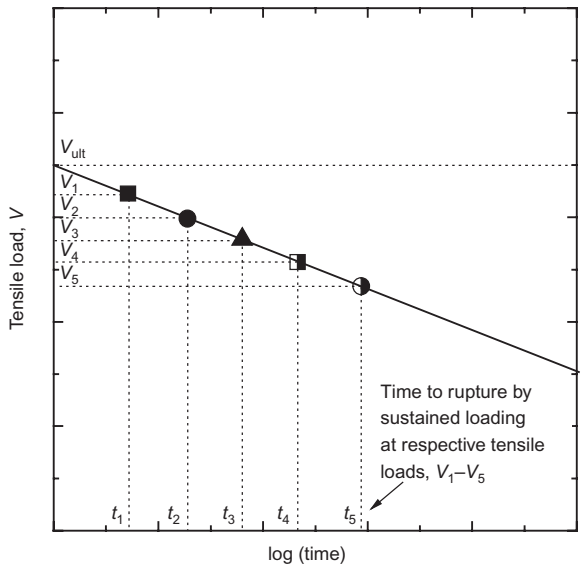

Figure 1. Schematic creep–rupture curve (not to scale)

multiple conventional creep tests of a given type of polymer geosynthetic reinforcement is generally high owing to the inevitable variance between different samples. For these reasons, Thornton *et al.* (1998) proposed another technique called 'the stepped isothermal method (SIM)'. By using the SIM technique, it is possible to obtain a master curve for a given tensile load V from a test using a single specimen, in which a series of separated isothermal dwell times are applied after respective stepwise increases in the temperature during sustained loading at the same tensile load (as explained later in this paper). Because of a smaller number of specimens needed and therefore a shorter test period, this technique is becoming increasingly popular in various countries for obtaining the stress-rupture curve (e.g. Baras *et al.* 2002; Thornton and Baker 2002; Zornberg & Kavazanjian 2002; Allen 2003; Greenwood *et al.* 2004; Narejo & Allen 2004; Zornberg *et al.* 2004; Bueno *et al.* 2005; Hsieh *et al.* 2006; Koo *et al.* 2006). Several researchers have reported that the time to creep rupture of geosynthetics predicted by the SIM technique agrees well with those actually measured by very long creep rupture tests (e.g. Greenwood *et al.* 2004; Bueno *et al.* 2005; Koo *et al.* 2006), even though the durations of these creep rupture tests are still far shorter than usual design life of, say, 50 years.

It is also true that, in both the TTS and SIM test procedures, the respective master curves for different tensile loads are obtained based on a set of 'shift factors', which are usually determined in a fairly empirical way. Moreover, no relevant constitutive model that can simulate the whole temperature sensitivity of creep strain rate observed in these two techniques as well as that in the field can be found in the literature. For this reason, no attempt has been made to understand the relationships between the consequences of the two methods on a consistent theoretical basis.

The deformation and strength characteristics of polymer geosynthetic reinforcement are basically elasto-viscoplastic, and thus are rate-dependent. Creep deformation of polymer geosynthetic reinforcement is merely a response due to its viscous properties, not a degrading phenomenon (e.g. Hirakawa *et al.* 2003; Kongkitkul *et al.* 2004a, 2007; Tatsuoka *et al.* 2004). Long-term deterioration of the intrinsic load–strain property by chemical and/or biological reactions is another phenomenon, called the 'negative ageing effect'. The effects of temperature increase on the strength and deformation characteristics of geosynthetics are equivalent to those of the negative ageing effects in decreasing the strength and stiffness. Therefore creep deformation that takes place at the same load but at different temperatures in TTS and SIM tests should be analysed by taking into account the effects of (1) rate effects due to viscous properties and (2) negative changes in the intrinsic tensile load–strain properties with temperature increase.

In this study, a nonlinear three-component constitutive model that can take into account the effects of these two factors was developed by extending the work by Kongkitkul *et al.* (2005). First, the model was used in direct simulations of long-term (i.e. 50 years) sustained loading (SL) at different applied tensile loads at the reference temperature. Then the same model was used to simulate the load–strain–time behaviour during SL at different tensile loads and different temperatures applied in *numerical* TTS and SIM tests. The master curves for different applied sustained tensile loads were then obtained from these numerical TTS and SIM tests based on the empirical methods suggested by GRI (2000) and then compared with the creep strain–log(time) relations that were obtained from the direct simulations. Then the creep–rupture curves, as illustrated in Figure 1, were obtained from these sets of creep strain–log(time) relations from the direct simulations as well as master curves from these numerical TTS and SIM tests. The numerical TTS and SIM tests based on the proposed constitutive model are also relevant to other procedures (e.g. ASTM D6992). The results from the numerical TTS and SIM tests were also interpreted based on ASTM D6992 to obtain master curves that are slightly different from those explained above.

Thornton *et al.* (1998), Greenwood *et al.* (2004) and Bueno *et al.* (2005), among others, have shown that the TTS and SIM tests are most relevant to polypropylene (PP), low-density polyethylene (LDPE) and polyester (PET). However, the numerical TTS and SIM tests described in this paper were not aimed at analysis of the behaviour of any specific type of geosynthetic reinforcement product. Rather, this paper aims mainly at introducing a constitutive model that has a framework relevant to the analysis of TTS and SIM tests of any given type of polymer geosynthetic reinforcement. It is shown in this paper that, although it is necessary to validate the model based on relevant experimental data, the model has the potential to predict the load–strain relation of polymer geosynthetic reinforcement subjected to arbitrary histories of load (or strain) and temperature together with their rates in load–strain tests, as well as model tests in the laboratory and full-scale field cases.

2. CONSTITUTIVE MODELLING

2.1. Modelling of elasto-viscoplastic properties

Figure 2 shows the non-linear three-component model that was first developed to simulate the elasto-viscoplastic stress–strain behaviour of geomaterials (i.e. soils and rocks) (e.g. Di Benedetto *et al.* 2002; Tatsuoka *et al.* 2002). The model was then modified to simulate the load–strain behaviour of geosynthetic reinforcement (Hirakawa *et al.* 2003; Kongkitkul *et al.* 2004a, 2007; Tatsuoka *et al.* 2004). Here, the tensile load is represented by V, not T, because T is used to represent temperature in this paper. The tensile load, V, is separated into the inviscid and viscous load components, V^{f} and V^{v}, and the tensile strain rate, $\dot{\varepsilon}$, into the elastic and irreversible (i.e. inelastic or viscoplastic) components, $\dot{\varepsilon}^{\mathrm{e}}$ and $\dot{\varepsilon}^{\mathrm{ir}}$. Elastic strain rates are obtained based on the hypo-elastic model $\dot{\varepsilon}^{\mathrm{e}} = \dot{V}/E_{\mathrm{eq}}(V)$, where $E_{\mathrm{eq}}(V)$ is the elastic modulus, which is a function of the instantaneous tensile load V. In this study $E_{\mathrm{eq}} = 5000$ kN/m was assumed constant.

When the current viscous load component V^{v} depends on instantaneous irreversible strain and its rate, and the tensile strength developed during ML increases with an increase in the strain rate, the viscous property is referred to as the *isotach* type. Most of the geosynthetic reinforcement types that were tested by Hirakawa *et al.* (2003), Shinoda and Bathurst (2004) and Kongkitkul *et al.* (2007) exhibit isotach viscosity. Isotach viscosity was also assumed in the simulations in this paper. The experimental results showed that, for the isotach viscosity, the value of V^{v} for a given value of $\dot{\varepsilon}^{\mathrm{ir}}$ is always proportional to the inviscid load V^{f}, obtained as

$$V^{\mathrm{v}}_{\mathrm{iso}} = V^{\mathrm{f}}\, g_{\mathrm{v}}(\dot{\varepsilon}^{\mathrm{ir}}) \tag{1}$$

where $g_{\mathrm{v}}(\dot{\varepsilon}^{\mathrm{ir}})$ is the viscosity function. In the present study, the following non-linear function of $\dot{\varepsilon}^{\mathrm{ir}}$ that has been proposed for geomaterials (Di Benedetto *et al.* 1999) was used

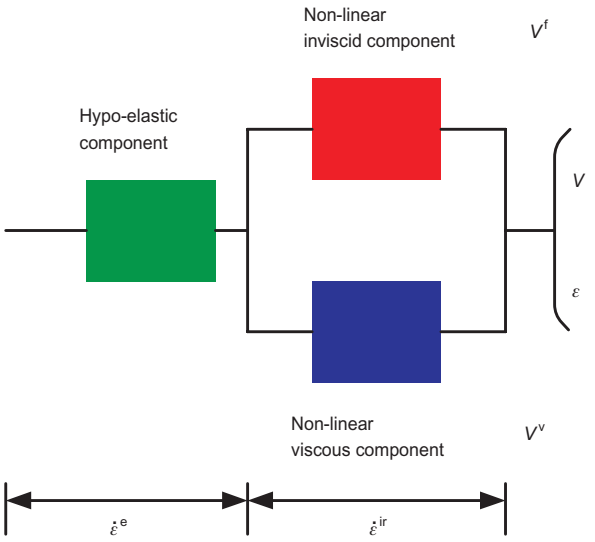

Figure 2. Non-linear three-component model for geosynthetic reinforcement (Hirakawa *et al.* 2003; Kongkitkul *et al.* 2004a)

$$g_{\mathrm{v}}(\dot{\varepsilon}^{\mathrm{ir}}) = \alpha^* \left(\dot{\varepsilon}^{\mathrm{ir}}/\dot{\varepsilon}^{\mathrm{ir}}_0\right)^{1+b^*} \tag{2}$$

where α^*, b^* and $\dot{\varepsilon}^{\mathrm{ir}}_0$ are the material constants. The parameters $\alpha^* = 0.36$, $1 + b^* = 0.16$ and $\dot{\varepsilon}^{\mathrm{ir}}_0 = 10^{-3}$ %/s were selected. These parameters are relevant in representing the viscous properties of most polymer geosynthetic reinforcements (Tatsuoka *et al.* 2006). Equation 2 is different from the equation used to analyse the load–strain–time behaviour of geosynthetic reinforcement in tensile loading tests including short-term sustained loading (Hirakawa *et al.* 2003; Kongkitkul *et al.* 2004a). In the present study, Equation 2 was used to simulate the creep behaviour during long-term sustained loading in which the strain rate becomes extremely low, because Equation 2 becomes more relevant as the strain rate becomes lower. Kongkitkul *et al.* (2007) showed that the model (Figure 2) incorporating Equation 2 can properly simulate:

- different V–ε curves from continuous ML tests at constant but different $\dot{\varepsilon}$;
- load jumps upon a stepwise increase/decrease in $\dot{\varepsilon}$ during otherwise ML;
- creep strains during sustained loading at constant load lasting for up to 30 days;
- load relaxation.

Furthermore, the model has been incorporated into an FEM code to account for the viscous properties of geomaterials (i.e. soils and rocks) as well as geosynthetic reinforcements. The behaviour of geosynthetic-reinforced soil structures observed in physical model tests was successfully simulated by the elasto-viscoplastic FEM analysis (e.g. Kongkitkul *et al.* 2004b; Tatsuoka *et al.* 2004; Noguchi *et al.* 2006; Siddiquee *et al.* 2006).

2.2. Modelling for ageing effects and temperature change effects

2.2.1. *Ageing effects*

Tatsuoka *et al.* (2003) and Di Benedetto *et al.* (2005) modified the above-mentioned non-linear three-component model to account for the ageing effects (both positive, such as cementation, and negative, such as weathering). The negative ageing effects (i.e. time-dependent degradation effects) on geosynthetic reinforcements by chemical and/or biological reactions when used in the field are taken into account by introducing the so-called 'reduction factor for degradation', RF_{D} to obtain the long-term design tensile strength in the practical procedure. In this study, the effects of time-dependent ambient temperature increase were dealt with as a kind of negative ageing effect. With such ageing effects, the inviscid tensile load V^{f} becomes a function not only of instantaneous irreversible strain $\varepsilon^{\mathrm{ir}}$, but also time of t_{c} (having a fixed origin that is defined at the start of temperature change, not the general time). Then the current value of V^{f} is obtained as

$$[V^{\mathrm{f}}]_{(\varepsilon^{\mathrm{ir}},t_{\mathrm{c}})} = \int_{\tau=\varepsilon^{\mathrm{ir}}_1,t=t_{c1}}^{\varepsilon^{\mathrm{ir}},t_{\mathrm{c}}} [\mathrm{d}V^{\mathrm{f}}]_{(\tau,t)} \tag{3}$$

where $[\mathrm{d}V^{\mathrm{f}}]_{(\tau,t)}$ is the inviscid load increment that devel-

ops or shrinks when the time t_c is equal to t and the irreversible strain is τ, and ε_1^{ir} and t_{c1} are ε^{ir} and t_c at the start of loading where $V^f = 0$. Yielding of the inviscid load V^f is defined as the development of $d\varepsilon^{ir} > 0$, which takes place when the following conditions are satisfied:

$$[V^f]_{(\tau,t)} = \left[V_y^f\right]_{(\tau,t)} \text{ and } [dV^f]_{(\tau,t)} = [dV_y^f]_{(\tau,t)} \tag{4}$$

where V_y^f is the yield inviscid load that is subjected to ageing effects. The yield inviscid load increment $[dV_y^f]_{(\tau,t)}$ for a given step of loading from the moment when $\varepsilon^{ir} = \tau$ and $t_c = t$ to the moment when $\varepsilon^{ir} = \tau + d\tau$ and $t_c = t + dt$ consists of the following two components (Figure 3):

- a component by an irreversible strain increment, $d\tau$, while $dt = 0$, $[d\tau]_{dt=0}$;
- the other by a time increment dt, while $d\tau = 0$, $[dt]_{d\tau=0}$.

By the second term, even under non-yielding conditions, $[dV_y^f]_{(\tau,t)}$ develops by positive ageing effects and shrinks by negative ageing effects. Tatsuoka *et al.* (2003) proposed formulating $[dV_y^f]_{(\tau,t)}$as

$$\begin{aligned}\left[dV_y^f\right]_{(\tau,t)} &= \left[E^f\left(\varepsilon^{ir},\, t\right)\right]_{(dt=0)}d\tau + \left[F^f\left(\varepsilon^{ir},\, t\right)\right]_{(d\varepsilon^{ir}=0)}dt \\ \left[E^f\left(\varepsilon^{ir},\, t\right)\right]_{(dt=0)}d\tau &= E_0^f(\tau)A^f[t(\tau)]d\tau \\ \left[F^f\left(\varepsilon^{ir},\, t\right)\right]_{(d\varepsilon^{ir}=0)}dt &= \left\{a^f V_0^f[\tau(t)] + b^f\right\}\alpha^f(t)dt\end{aligned} \tag{5}$$

where $A^f(t_c)$ is the ageing function for V_y^f, which increases and decreases with an increase in t_c for positive and negative ageing effects, respectively, from $A^f(t_c = 0) = 1.0$; E_0^f is the basic tangent stiffness, independent of any ageing effects; a^f and b^f are constants; and $\alpha^f(t_c)$ is a function of t_c. The current value of V_y^f is obtained by integrating Equation 5 as

$$\begin{aligned}\left[V_y^f\right]_{(\varepsilon^{ir},t_c)} = V_0^f(\varepsilon^{ir}) &+ \int_{\tau=\varepsilon_1^{ir}}^{\varepsilon^{ir}}\left[E_0^f(\tau)\left\{A^f[t(\tau)] - 1.0\right\}\right]d\tau \\ &+ \int_{t=t_{c1}}^{t_c}\left[\left\{a^f V_0^f[\tau(t)] + b^f\right\}\alpha^f(t)\right]dt\end{aligned} \tag{6}$$

where $V_0^f(\varepsilon^{ir}) = \int_{\tau=\varepsilon_1^{ir}}^{\varepsilon^{ir}} E_0^f(\tau)d\tau$ is the inviscid yield load, which is independent of ageing effects. When $a^f = b^f = 0$, we obtain $A^f(t_c) \equiv 1.0$, and then $[V_y^f]_{(\varepsilon^{ir},t_c)}$ becomes $V_0^f(\varepsilon^{ir})$. When $a^f = 1.0$, $b^f = 0$ and $\alpha^f(t_c) = \partial A^f(t_c)/\partial t$, V_y^f becomes independent of loading history as follows:

$$\left[V_y^f\right]_{(\varepsilon^{ir},t_c)} = V_y^f\left(\varepsilon^{ir},\, t_c\right) = V_0^f(\varepsilon^{ir})A^f(t_c) \tag{7}$$

Equation 7 was assumed in this study. For $V_0^f(\varepsilon^{ir})$, the following non-linear relation was assumed:

$$V_0^f = \sum_{i=1}^{7} a_i(\varepsilon^{ir})^{i-1} \tag{8}$$

where V_0^f is in kN/m and ε^{ir} is in per cent. The shape of the load–strain curves during ML at constant strain rate and temperature (as shown later in Figure 9) is proportional to that given by Equation 8. Table 1 summarises the parameters used in Equation 8.

2.2.2. *Temperature increase effect*

Modelling of the temperature change effects was based on Equation 7. To this end, the ageing function for V_y^f, A^f, is first described as a function of the ambient temperature T as $A^f = f_2(T)$, where $A^f = f_2(T_1) = 1.0$, and T_1 is the reference temperature. Here T has a specified unit (e.g. degrees Celsius). In the present study $A^f = f_2(T)$ was represented by

$$\begin{aligned}A^f(T,\, \Delta T) &= \left[\frac{\exp(-0.2) + 1}{2}\right]^{(T-T_1)/\Delta T} \\ &\simeq 0.90937^{(T-T_1)/\Delta T}\end{aligned} \tag{9}$$

where T_2 to T_5 are higher ambient temperatures, and ΔT is a fixed positive temperature increase: that is,

$$\begin{aligned}T_2(= T_1 + \Delta T) &< T_3(= T_1 + 2\Delta T) \\ &< T_4(= T_1 + 3\Delta T) \\ &< T_5(= T_1 + 4\Delta T)\end{aligned}$$

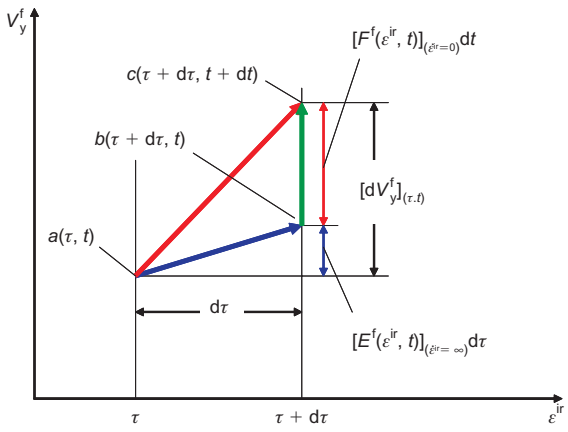

Figure 3. Yield inviscid tensile load increment dV_y^f, developed by increments of irreversible strain and time when both viscous and ageing effects are active (Tatsuoka *et al.* 2003)

Table 1. List of parameters used in Equation 8

a_1	a_2	a_3	a_4	a_5	a_6	a_7
0	11.1	−3.46	7.86×10^{-1}	-9.44×10^{-2}	5.61×10^{-3}	-1.3×10^{-4}

With an increase in T from T_1 to T_2, T_3, T_4 and finally T_5, $A^f = f_2(T)$ (Equation 9) successively decreases from 1.0, as shown in Figure 4.

Equation 9 (or another relevant functional form) for a given type of polymer geosynthetic reinforcement can be calibrated by using experimental data from continuous ML tests at a constant strain rate performed at different ambient temperatures (as presented later in Figures 9a and 9b). However, such data as above that are sufficient to this end cannot be found in the literature as far as the authors are aware. For this reason, only numerical TTS and SIM tests were performed in this study, not including any analysis of experimental data.

For a given time history of temperature, $T = f_1(t_c)$, the ageing function in terms of the time t_c is obtained by substituting $T = f_1(t_c)$ into $A^f = f_2(T)$ as $A^f = f_2[f_1(t_c)] = A^f(t_c)$. The ageing function $A^f(t_c)$ describes the effects of ambient temperature changes as a time-dependent degrading process (i.e. negative ageing effects). In the present study, for a temperature increase from T_1 to T_2, the following specific form was assumed for the function $A^f(t_c)$, referring to Equation 9:

$$A^f(\Delta t) = \frac{\exp(-\Delta t/50) + 1}{2} \tag{10}$$

where Δt is the time increment in seconds from the start of the increase in T. When applying Equation 10 to the temperature elevation processes in the numerical TTS and SIM tests (as described below), it was assumed that $\Delta t = 0$ and 10 s at the start and end of the temperature elevation from T_1 to T_2, for consistency with Equation 9. It was assumed that the elastic property and the viscosity function (Equation 2) do not change with changes in T.

3. SIMULATION

3.1. Direct simulations for 50-year sustained loading

Figure 5 shows the V–ε relations for ML at a strain rate of 1.0 %/min followed by 50-year SL at different levels of tensile load V equal to 32, 34, 36, 38 or 40 kN/m at a fixed temperature equal to the reference value T_1, which were obtained by direct simulations based on the nonlinear three-component model (Figure 2). In this case, the intrinsic property (i.e. the V^f–ε^{ir} relation) does not change with time, owing to the fixed ambient temperature.

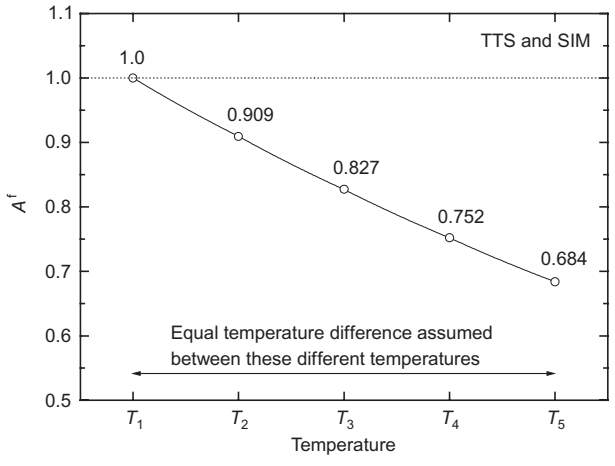

Figure 4. Ageing function A^f introduced to describe the effects of increase in the ambient temperature, T

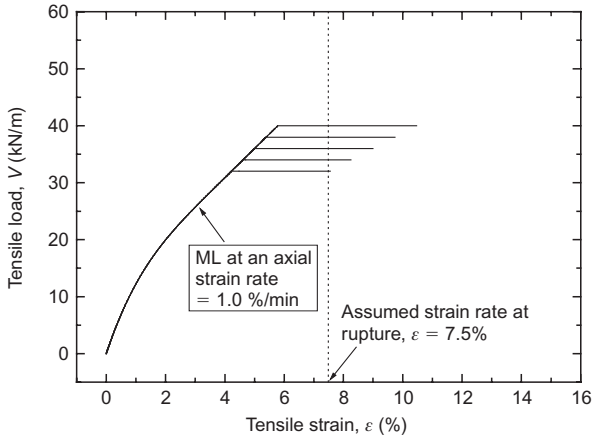

Figure 5. Tensile load–strain curves for continuous ML at a constant strain rate followed by sustained loading for 50 years (at a constant temperature T_1)

Hereafter, the creep tensile strain is defined as zero at the start of tensile loading (when $V = 0$), and the creep modulus is defined as the tensile load during SL divided by the tensile strain, defined as zero when $V = 0$. Figures 6a and 6b show, respectively, the relationships between creep strain and log(time), and between creep modulus and log(time), obtained by direct simulation of SL at $V =$ 32 kN/m (the results from the numerical TTS and SIM tests presented in these figures are explained later). Similar results obtained for SL at $V = 40$ kN/m are presented in Figures 7a and 7b.

3.2. Time–temperature superposition (TTS) method

A set of numerical TTS tests was performed in which continuous ML at a constant strain rate equal to 1.0 %/min was applied following the time histories of tensile strain shown in Figure 8a. Then sustained loading (SL) for 1 h (i.e. 3600 s) was applied at a constant tensile load, V, equal to 32, 34, 36, 38 or 40 kN/m during otherwise ML. These tensile loads were selected rather arbitrarily, and not related to the specific ultimate tensile rupture strength. In fact, the proposed model is general and can be applied to any sustained loads with any rupture strength. It is not an objective of this study to analyse the effects of sustained tensile load on the creep deformation behaviour.

Figure 8b shows how $A^f(t_c)$ was set to change with time by temperature increase at $V = 0$ from $T = T_1$ at $t_c = 0$ until $T = T_5$ at $t_c = 40$ s. The times that had elapsed by the start of ML at temperatures equal to T_1 (the reference value), T_2, T_3, T_4 and T_5 were, respectively, $t_c = 0$, 10, 20, 30 and 40 s. The effects of temperature increase from the reference value T_1 to another, T, at $V = 0$ were represented by an increase of t_c in $A^f(t_c)$ (Equation 10). For example, before the start of ML at T_3, $A^f(t_c)$ had decreased at $V = 0$ from 1.0 to $[\exp(-10/50) + 1]/2 = 0.909$ for the first 10 s and then to $\{[\exp(-10/50) + 1]/2\}^2 = 0.827$ for the next 10 s. The value of $A^f(t_c)$ was then kept constant during

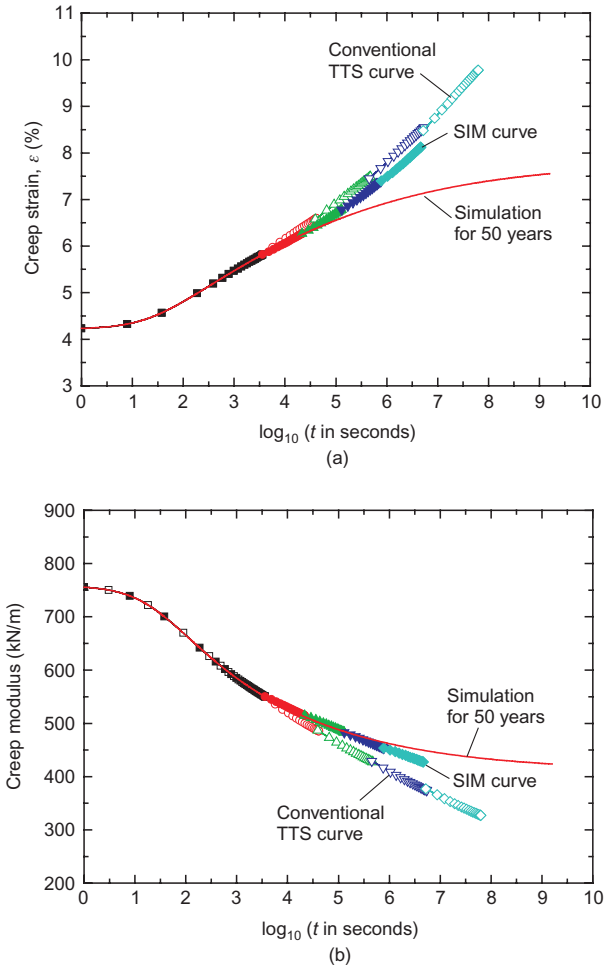

Figure 6. (a) Creep strain against log(time) relations and (b) creep modulus against log(time) relations for sustained loading at $V = 32$ kN/m from direct simulation, plus master curves obtained by numerical TTS and SIM tests

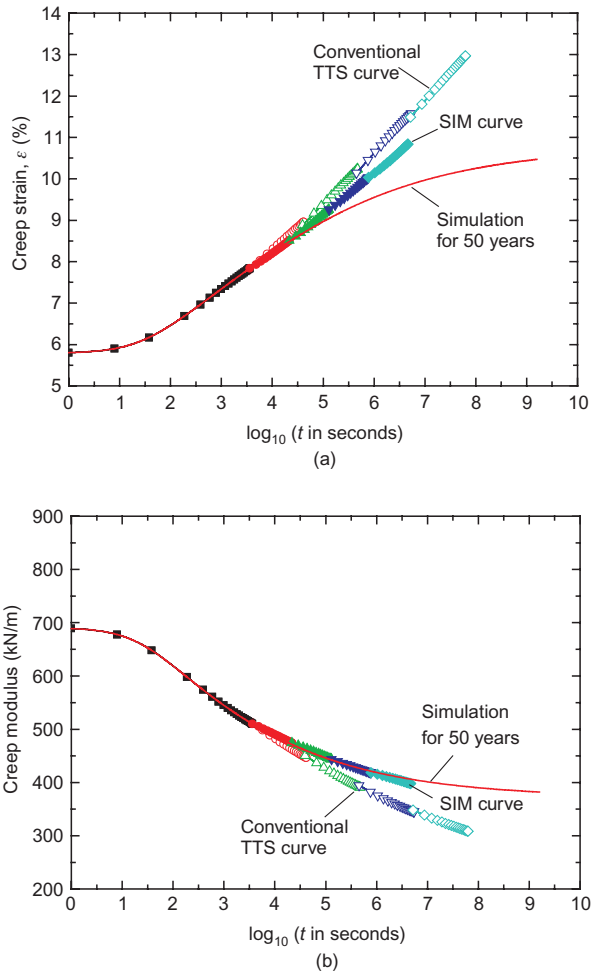

Figure 7. (a) Creep strain against log(time) relations and (b) creep modulus against log(time) relations for sustained loading at $V = 40$ kN/m from direct simulation, plus master curves obtained by numerical TTS and SIM tests

subsequent ML and SL at the same temperature, T_1, T_2, T_3, T_4 or T_5.

Figures 9a and 9b show the V–ε curves obtained by the numerical TTS tests performed following the time histories of strain and temperature presented in Figures 8a and 8b. In these tests, continuous ML was followed by SL at $V = 32$ kN/m and 40 kN/m. The V–ε relations at higher temperatures exhibit lower stiffness as a result of the introduction of $A^{\mathrm{f}}(t_{\mathrm{c}}) \leqslant 1.0$.

Figures 10a and 10b show, respectively, the time histories of creep strain during SL at $V = 32$ and 40 kN/m at different temperatures, corresponding to Figures 9a and 9b. The corresponding time histories of creep modulus are presented in Figures 11a and 11b. The horizontal axis of Figures 10 and 11 is the logarithm of the elapsed time in seconds, defined as zero at the start of SL. It can be seen that, with an increase in the temperature, the creep strain rate increases while the creep modulus decreases; both effects are due to a decrease in the stiffness of the V^{f}–$\varepsilon^{\mathrm{ir}}$ relation associated with an increase in the ambient temperature. This trend of behaviour is consistent with experimental data reported by Hirakawa *et al.* (2003) and Kongkitkul *et al.* (2007) that, for the same initial strain rate at the start of SL, the creep strain rate of a given type of geosynthetic reinforcement increases with a decrease in the tangent stiffness at the sustained load of the load–strain relation by ML at a constant strain rate.

The vertical dashed lines in Figures 10 and 11 indicate an elapsed time of 300 s since the start of SL. It may be seen that all the relations appear to become linear after this point. Each set of these apparently linear relations, truncated for elapsed time longer than 300 s for different temperatures at the same tensile load, were shifted to the right and overlapped to form a single smooth continuous curve, as shown in Figures 6 and 7. This procedure is one of the key steps of the TTS technique. The use of apparently truncated linear relations at this step, as shown above, follows the method that is usually used (e.g. Thornton *et al.* 1998). In practice, it is not possible to obtain smooth continuous curves, such as those shown in Figures 6 and 7, by lateral shifting and overlapping of the respective sets of the whole curves presented in Figures 10 and 11. The curves shown in Figures 6 and 7 refer to the master curves in terms of creep strain and creep modulus for SL when $V = 32$ and 40 kN/m obtained by the TTS technique. The amount of shifting of the respective sets of curves for the four different temperatures T_2 to T_5, shown in Figures 10 and 11, to the right along the axis of the

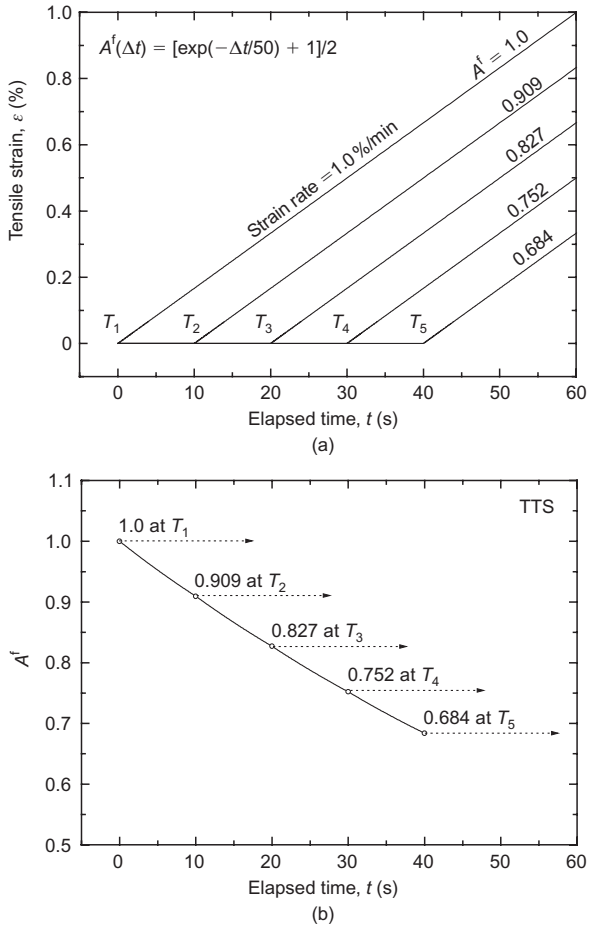

Figure 8. Time histories of (a) tensile strain and (b) A^f employed in the numerical TTS tests

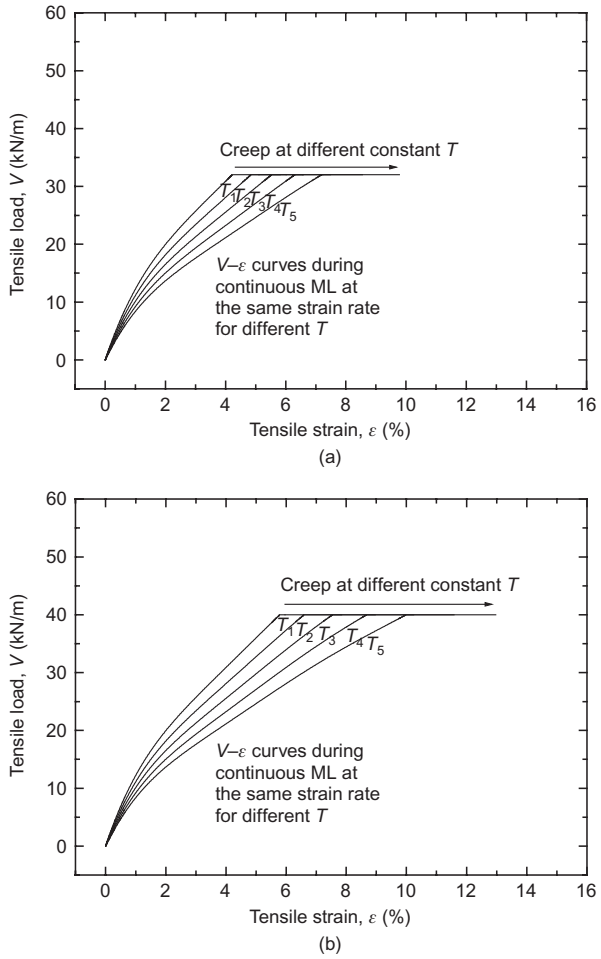

Figure 9. Tensile load–strain curves for continuous ML at a constant strain rate followed by sustained loading at (a) $V =$ 32 kN/m and (b) $V = 40$ kN/m, under different but constant temperatures from numerical TTS tests

logarithm of time is equal to 1.06, 2.12, 3.18 and 4.24, respectively. This lateral shift is equivalent to multiplication of the elapsed time for the respective sets of curves for the four different temperatures by factors of $10^{1.06}$, $10^{2.12}$, $10^{3.18}$ and $10^{4.24}$, respectively. By this method, the time range of creep strain/modulus curves was extrapolated from 3.56 log-cycles of time in the single SL tests at the initial/reference temperature T_1 (Figures 10 and 11) towards about 7.8 log-cycles, or from 1 h towards about 2 years (Figures 6 and 7).

3.3. Stepped isothermal method (SIM)

Figures 12a and 12b show the V–ε relations obtained by numerical SIM tests of SL tests at $V = 32$ and 40 kN/m. The tensile load and tensile strain rate at the start of SL in each case were set the same as those employed in the numerical TTS tests described above. During the respective SL stage at the fixed tensile load (i.e. at either $V =$ 32 or $V = 40$ kN/m), the ambient temperature T was increased stepwise four times while otherwise keeping the temperature constant for a duration of 3600 s. The inviscid load V^f decreases suddenly upon the respective stepwise temperature increase (Figures 12a and 12b). This response upon a step temperature increase was dealt with as negative ageing effects and taken into account based on the ageing function A^f (Equation 10). After a sudden decrease upon each step temperature increase, the inviscid load V^f gradually increases with an increase in the irreversible tensile strain ε^{ir}, following the new degraded inviscid tensile load–strain relation for a constant higher temperature. Abrupt degradation of the V^f–ε^{ir} relation upon a temperature increase results in a sudden acceleration of creep strain rate, as shown below.

Figure 13 compares the V–ε curves from these numerical SIM tests in which SL was performed at $V = 32$, 34, 36, 38 and 40 kN/m with those from numerical continuous ML tests performed at the same constant strain rate (i.e. 1.0 %/min) under constant but different temperatures, T_1, T_2, T_3, T_4 and T_5. The V–ε curves after ML is restarted at the end of each SL where $T = T_5$ in the numerical SIM tests rejoin the curve obtained by continuous ML at the constant temperature T_5. This trend of behaviour results from the use of Equation 1 (i.e. the isotach viscosity) and Equation 7 (i.e. the ageing effects or the temperature change effects on the inviscid tensile load, V^f, are independent of loading history). That is, when based on Equations 1 and 7, a unique viscous load V^v is obtained for given instantaneous values of irreversible strain, its rate and temperature, irrespective of previous histories of strain and temperature.

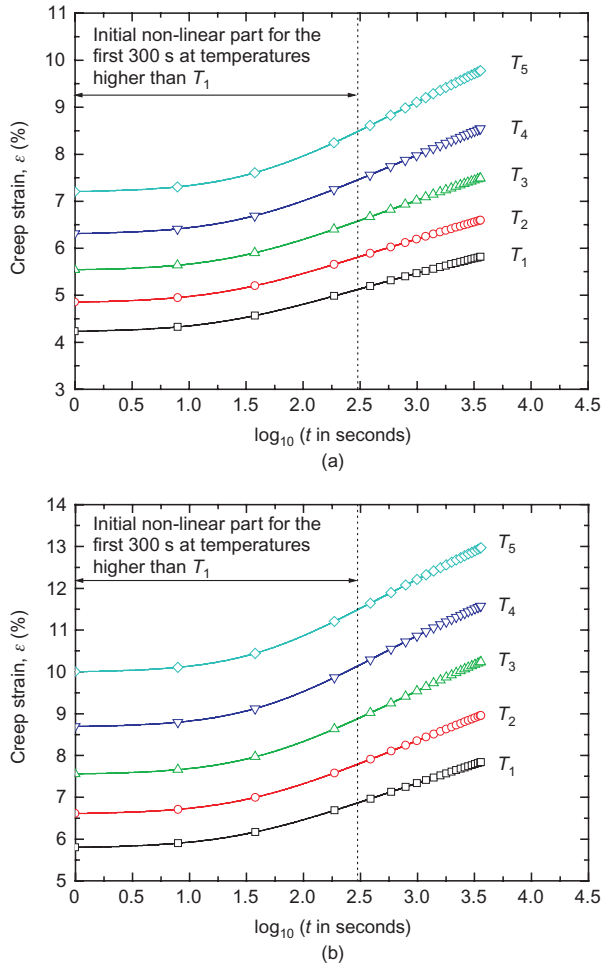

Figure 10. Time histories of creep strain by numerical TTS tests: (a) $V = 32$ kN/m; (b) $V = 40$ kN/m

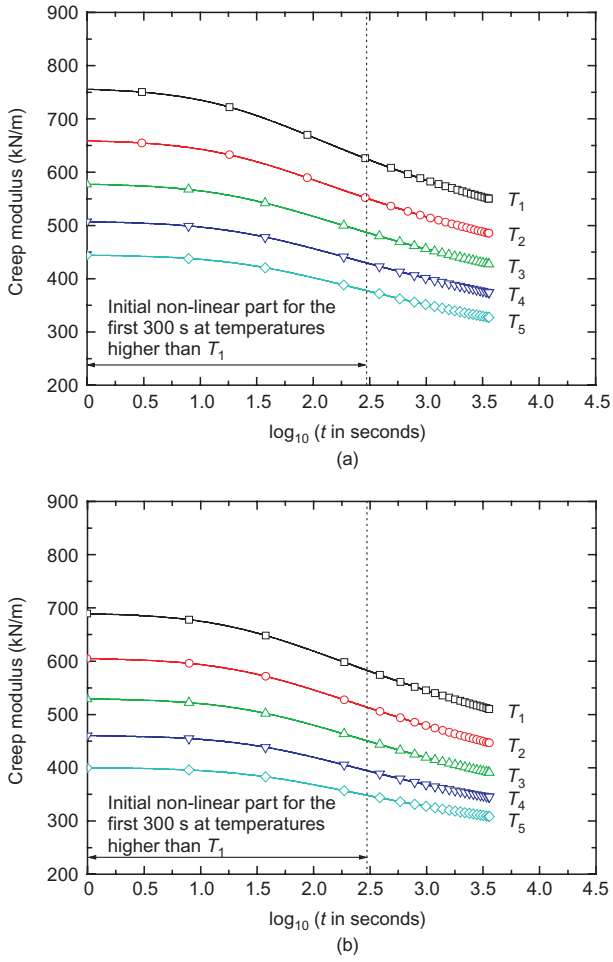

Figure 11. Time histories of creep modulus by numerical TTS tests: (a) $V = 32$ kN/m; (b) $V = 40$ kN/m

Figures 14a and 14b show the time histories of total and inviscid tensile loads, V and V^f, during SL at $V = 32$ and 40 kN/m obtained from the numerical SIM tests. Figures 15a and 15b show part of Figures 14a and 14b before, during and after the transition from T_1 to T_2. That is, $A^f(t_c)$ was kept equal to 1.0 during the initial continuous ML stage and the first 3600 s of the subsequent SL at T_1. Then the temperature T was increased at a constant rate for a duration of 10 s, which resulted in a fast decrease in $A^f(t_c)$ from 1.0 to 0.909, following Equation 10, which was maintained during SL at T_2 for the next 3590 s. The transitions of $A^f(t_c)$ when the temperature was increased from T_2 to T_3, from T_3 to T_4 and from T_4 to T_5 were made following Equation 10 in the same way as that from T_1 to T_2.

Figures 16a and 16b show the time histories of the total and irreversible tensile strains, ε and ε^{ir}, corresponding to Figures 14a and 14b. The creep strain rate suddenly increases by a step temperature increase, whereas it decreases gradually with time during any subsequent SL at a fixed temperature. These trends of behaviour are consistent with those obtained by actual SIM tests (e.g. Thornton *et al.* 1998; GRI 2000; Zornberg *et al.* 2004; Bueno *et al.* 2005).

Figures 17a and 17b show the corresponding time histories of creep strain, where t is the time that has elapsed since the start of SL at T_1 and t' is the time that has elapsed until the start of the current SL stage at an elevated temperature. That is, $t - t'$ is the dwell time that has elapsed since the start of SL at the current elevated temperature. The corresponding time histories of creep modulus are presented in Figures 18a and 18b.

Following GRI (2000), the curves of creep strain and creep modulus against log(time) curves were redefined so that their slopes at the beginning of an elevated temperature dwell match those of the end of the respective curves at the preceding lower temperature. In the present study, this process was made by:

1. removing the initial non-linear part for a relevant period Δt_1 from the respective relations so that the initial slope of the remaining part of the curve at an elevated temperature becomes the same as that at the end of the preceding sustained loading at the lower temperature; and
2. vertically shifting the creep strain (and modulus) and log(time) curves obtained by step 1.

Figures 19 and 20 show the time histories of creep strain and creep modulus for SL at $V = 32$ and 40 kN/m obtained by applying these two-step procedures to the curves presented in Figures 17 and 18. $\Delta t_1 = 600$ s was

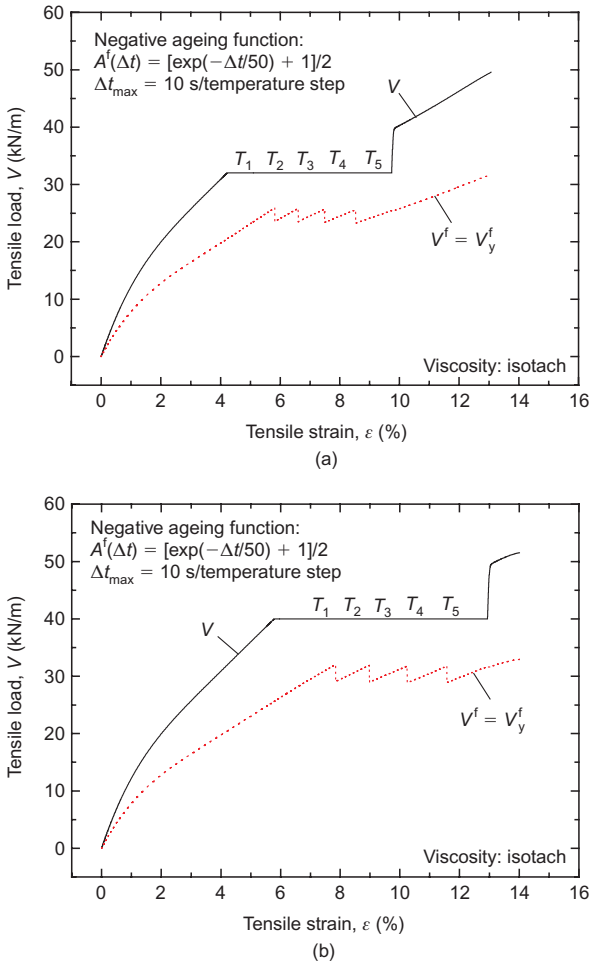

Figure 12. Tensile load–strain relations showing sudden decreases in the inviscid load upon stepwise increases in the temperature from numerical SIM tests for sustained loading at: (a) $V = 32$ kN/m; (b) $V = 40$ kN/m

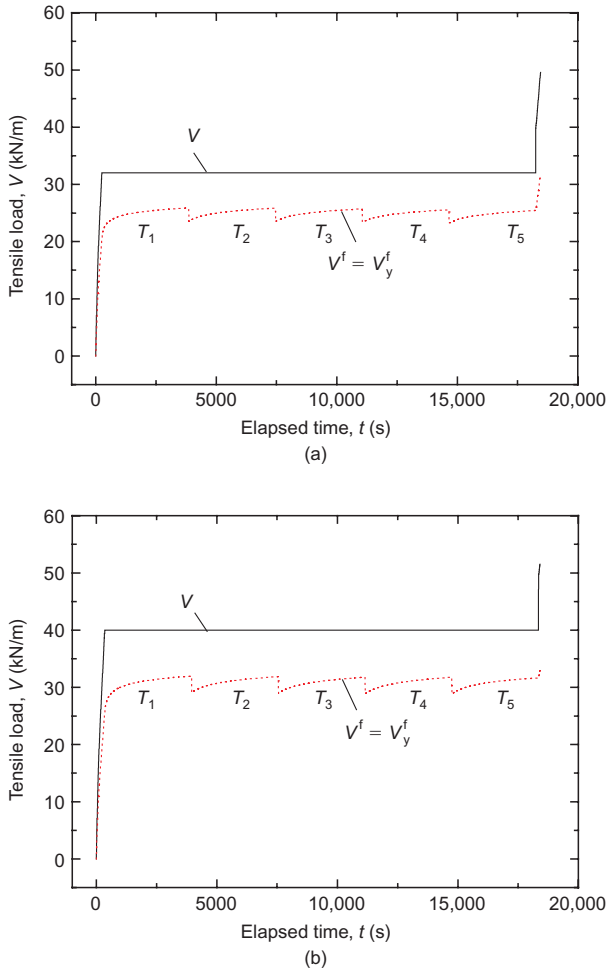

Figure 14. Time histories of V and V^f with sudden decreases in V^f upon step increases in the temperature during SL at (a) $V = 32$ kN/m, (b) $V = 40$ kN/m; numerical SIM tests

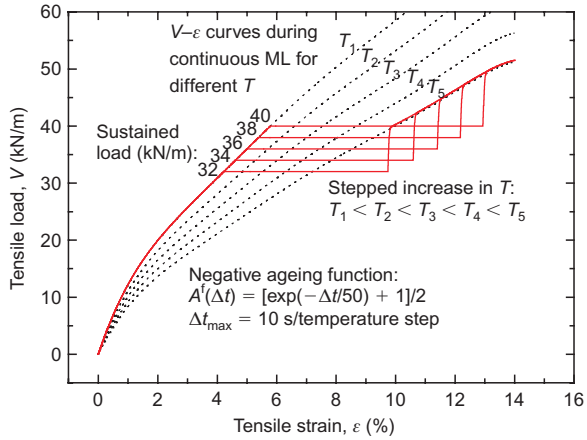

Figure 13. Comparison of tensile load–strain curves from numerical SIM tests and continuous ML tests at different but constant temperatures

selected in step 1 for all the SL stages at different V values. The master curves that are presented in Figures 6 and 7 were then obtained by horizontally shifting the curves presented in Figures 19 and 20 by a factor of 0.778. As may be seen from Figures 6 and 7, by this procedure, creep strain/modulus master curves for about 6.67 log-cycles of time were obtained, which largely exceed the range in the single SL tests at T_1.

Figures 21a and 21b show, respectively, the curves of creep strain and creep modulus against log(time) obtained for SL at $V = 32$ to 40 kN/m by the direct simulations. The master creep strain curves and the master creep modulus curves obtained at the respective loads by the numerical TTS tests are presented in Figures 22a and 22b. The similar results obtained by the numerical SIM tests are presented in Figures 23a and 23b.

3.4. Comparison of master curves by direct simulations and numerical TTS and SIM tests

It may be seen from Figures 6 and 7 and also by comparing Figures 21, 22 and 23 that, when $\log t$ (in seconds) < 4.0, the curves of creep strain and creep modulus against log(time) (i.e. the master curves) for the same SL level obtained from direct simulations of long-term SL at the reference temperature and the numerical TTS and SIM tests are very similar to each other. However, as $\log t$ becomes larger than around 4.0, the master curves from the direct simulations gradually become different from those from the numerical TTS and SIM tests. That is, for the same creep strain or modulus,

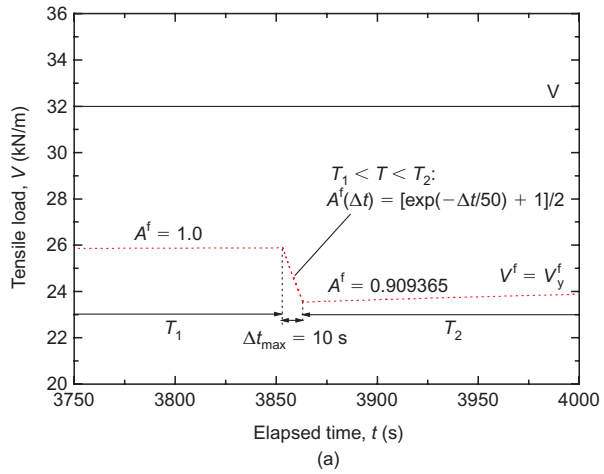

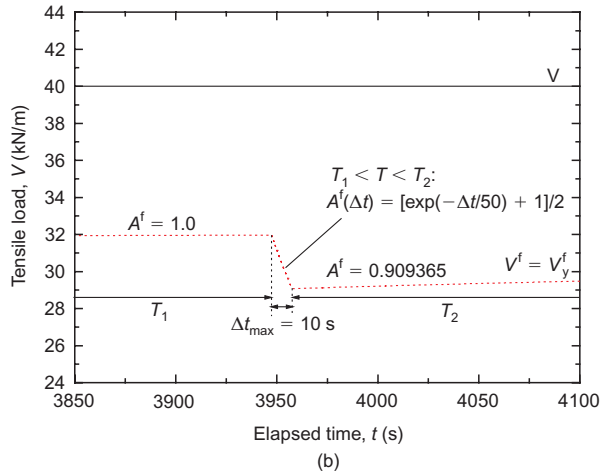

Figure 15. Enlarged part of Figures 14a and 14b where the temperature is increased stepwise from T_1 to T_2, SL at: (a) V = 32 kN/m; (b) V = 40 kN/m

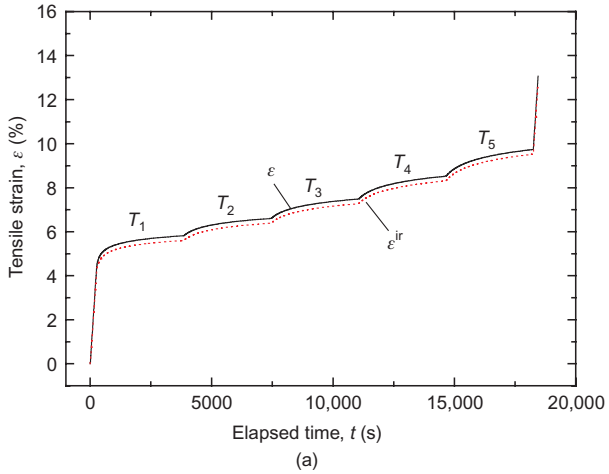

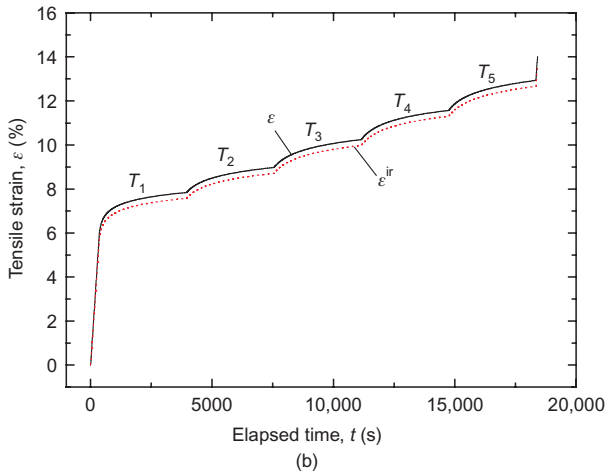

Figure 16. Time histories of total and irreversible tensile strains during SL at (a) V = 32 kN/m, (b) V = 40 kN/m; numerical SIM tests

the direct simulations exhibit longer creep rupture time. This may be due to the fact that, in the direct simulations using Equation 2, the increasing rate of tensile creep strain during SL decreases with time and eventually becomes very small, although not zero. Therefore in Figures 6a and 7a, where time is plotted using a logarithmic scale, the curves of creep strain against log(time) are linear until about $\log t < 4.5$ and then became concave downwards after $\log t > 4.5$. On the other hand, the master curves obtained from the numerical TTS and SIM tests reflect only the property of Equation 2 before the strain rate becomes very low. This is also the case with actual TTS and SIM tests performed to simulate long-term SL at a fixed temperature.

The master curves obtained from the numerical TTS and SIM tests are slightly different from each other, although they are very similar to each other when compared with those obtained by the direct simulations of long-term SL at the reference temperature. It seems that some differences seen for $\log t > 4.0$ are due partly to some inherent features of the specific time-rescaling procedure employed to obtain the master curves by the numerical SIM tests. Furthermore, it may be seen that the master creep modulus curve (Figures 6b and 7b) is slightly smoother than the master creep strain curve (Figures 6a and 7a) for both numerical TTS and SIM tests. This fact may explain why many researchers and engineers prefer the use of master creep modulus curves over master creep strain curves (e.g. Thornton *et al.* 1998; GRI 2000).

4. CREEP RUPTURE CURVES

4.1. Comparison of direct simulation, TTS and SIM techniques

The rupture strain increases with an increase in the ambient temperature under otherwise the same conditions (e.g. Zornberg and Kavazanjian 2002). On the other hand, Hirakawa *et al.* (2003) reported that, with all the geosynthetic reinforcement types used in a comprehensive series of tensile loading tests performed at essentially the same temperature, the strain at tensile rupture of each type of geosynthetic reinforcement was nearly the same irrespective of applied different pre-rupture loading histories and loading periods until rupture as well as largely different strain rates at rupture. Moreover, the master curves presented in Figures 22 and 23 are considered to be equivalent to the time histories of creep strain and

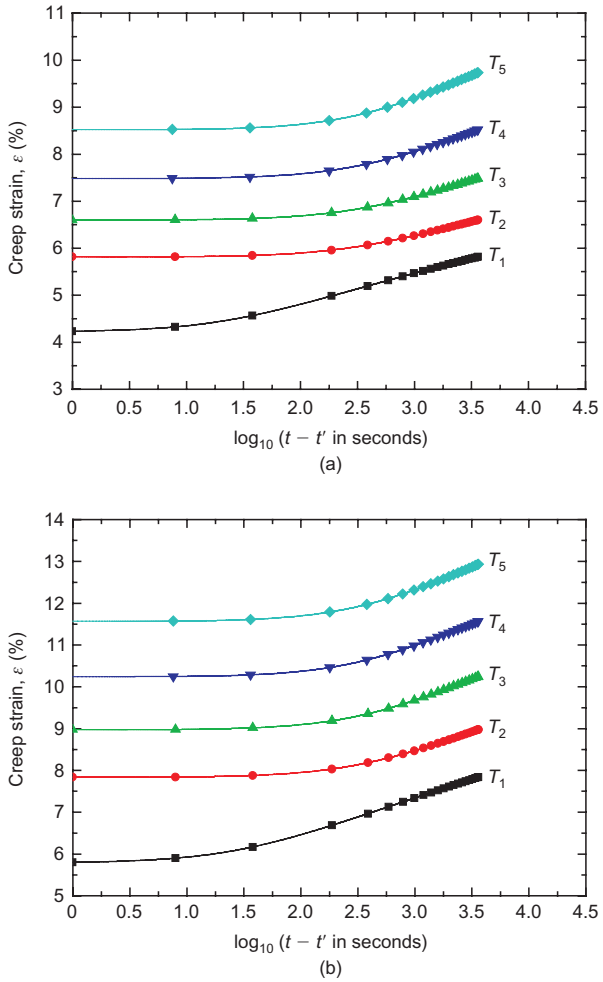

Figure 17. Time histories of creep strain at different temperatures during SL at (a) $V = 32$ kN/m, (b) $V = 40$ kN/m; numerical SIM tests

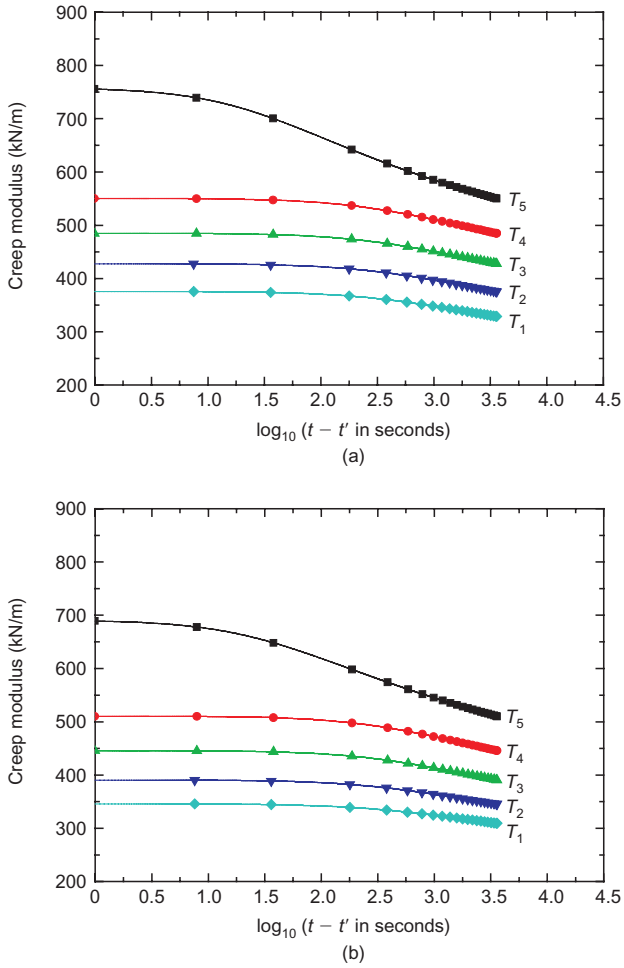

Figure 18. Time histories of creep modulus at different temperatures during SL at (a) $V = 32$ kN/m, (b) $V = 40$ kN/m; numerical SIM tests

modulus obtained from long-term SL under constant ambient temperature T equal to the reference temperature T_1, as presented in Figure 21.

For these reasons, in the present study, a fixed rupture tensile strain equal to 7.5% was assumed arbitrarily, as shown in Figures 21a, 22a and 23a. Note that the conclusions of the present study do not change when using other rupture strains. In Figures 21b, 22b and 23b a rupture strain of 7.5% has been converted to rupture creep moduli for the respective sustained loads. Then the elapsed time when the creep rupture takes place after the start of the respective SL was obtained. Finally, the relationships between the sustained load and the corresponding creep rupture time (i.e. the creep rupture curves) obtained by the direct simulations and the numerical TTS and SIM tests were obtained, as shown in Figure 24. The following trends of behaviour may be seen in Figure 24.

- The creep rupture curves obtained by the direct simulations and the numerical TTS and SIM tests are rather similar for $\log t$ (t in seconds) less than about 5. As $\log t$ becomes larger than about 5, the deviation between the curve obtained by the direct simulations and those from the numerical TTS and SIM tests becomes larger. This result suggests that the creep rupture strength obtained by the TTS and SIM tests on a given type of geosynthetic reinforcement could become more conservative with an increase in the creep rupture time when compared with that obtained directly by long-term SL at constant tensile loads.
- The creep rupture curves obtained by the numerical TTS and SIM tests are nearly linear compared with that obtained by the direct simulations. The difference between the two curves gradually increases with an increase in time.
- The creep rupture time for the same tensile load according to the direct simulations is longest, whereas that according to the numerical SIM tests is longer than that according to the numerical TTS tests.

The differences between the creep rupture curves described above result from differences between the master curves using the three methods. Figures 6 and 7 show that the time to reach the same strain at the

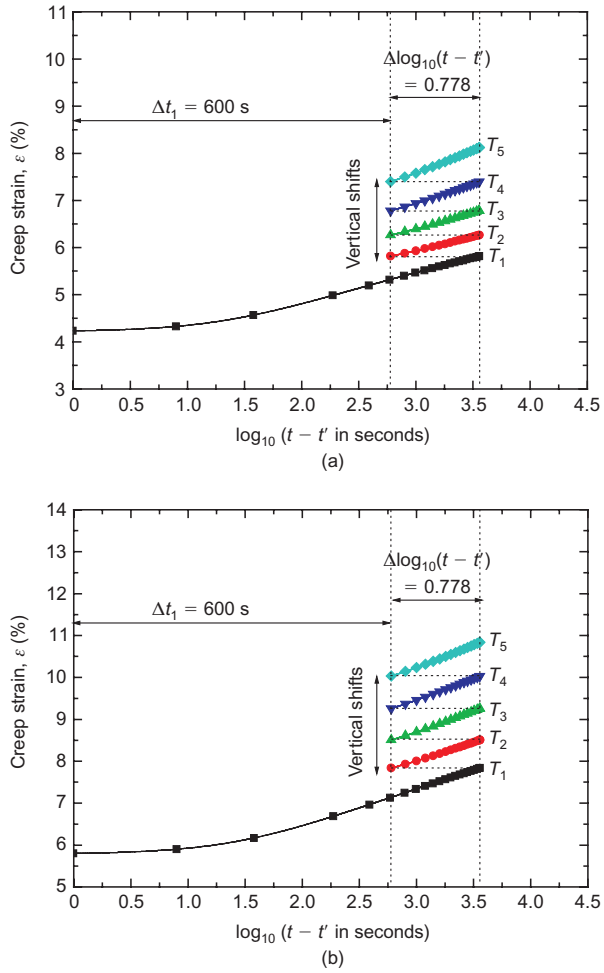

Figure 19. Creep strain–log(time) curves for SL at: (a) V = 32 kN/m; (b) V = 40 kN/m (after removing the initial part and vertical shifting of the curves presented in Figures 17a and 17b)

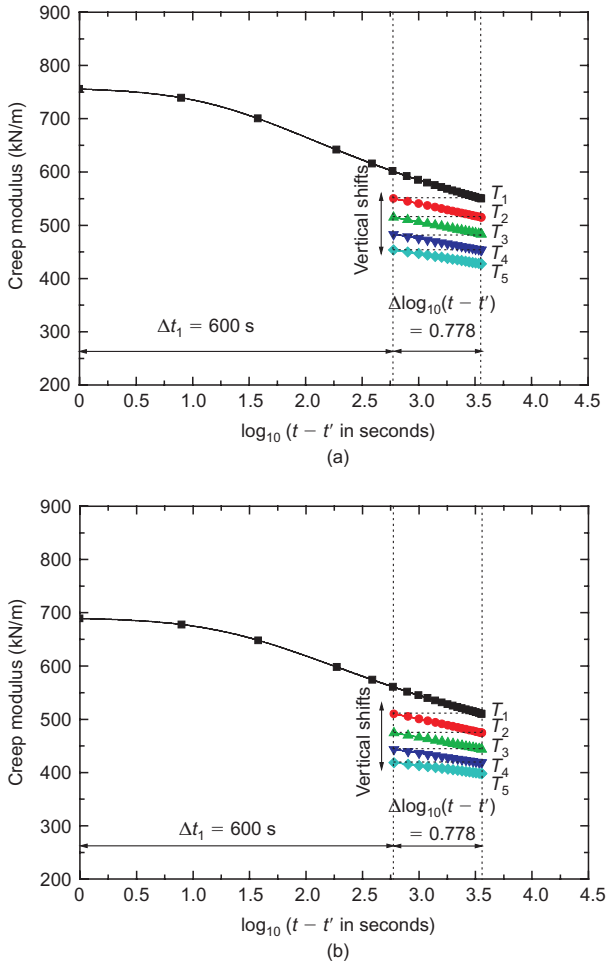

Figure 20. Creep modulus–log(time) curves for SL at: (a) V = 32 kN/m; (b) V = 40 kN/m (after removing the initial part and vertical shifting of the curves presented in Figures 18a and 18b)

respective SL stage becomes longer in the order of the direct simulations, the numerical SIM tests and the numerical TTS tests. More specifically, the differences are due to the following factors.

- The lowest strain rates encountered in the numerical TTS and SIM tests are significantly larger than those in the direct simulations of long-term SL, as discussed in the preceding section. Therefore the TTS and SIM techniques may not fully simulate the creep deformation process after some long time of SL at the reference ambient temperature.
- The procedures to obtain the master curves are inherently different between the TTS and SIM techniques. That is, the amounts of time rescaling and vertical shifting used to obtain the master curves are different between the numerical TTS and SIM tests and between the master curves in terms of creep strain and modulus; they are rather arbitrary, and not linked to each other.

It should also be recalled that, for the time histories of creep strain and modulus presented in Figures 10 and 11 from the numerical TTS tests and in Figures 17 and 18 from the numerical SIM tests, the time is defined as zero at the start of the respective SL and at the start of the step temperature increase, respectively. On the other hand, the time history of creep strain and modulus from the numerical TTS and SIM tests, the initial part in particular, is controlled by the initial creep strain rate, which is equal to the irreversible strain rate immediately before the start of SL and the start of the step temperature increase, respectively. Therefore the results from the TTS and SIM tests are influenced in different ways by the strain rate during ML before the start of SL (equal to 1.0 %/min) and by the accelerated strain rate upon the step increase in the temperature in the present case. This point also means that it is necessary to define and control the initial creep strain rates for objective results to be obtained from TTS and SIM tests. Therefore the differences seen between the creep rupture curves from the numerical TTS and SIM tests and between those based on the master creep strain and modulus curves from numerical SIM tests seen in Figure 24 are *not* general.

4.2. Discussion

The creep strain/modulus–log(time) curves and master curves presented in Figures 21, 22 and 23 were obtained

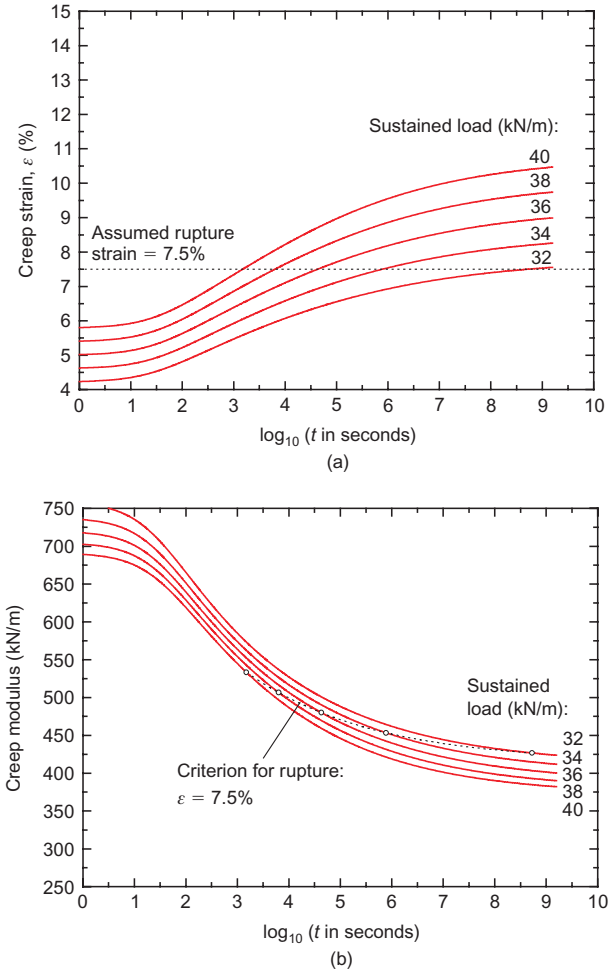

Figure 21. (a) Creep strain–log(time) curves and (b) creep modulus–log(time) curves, obtained from direct simulations of SL for 50 years

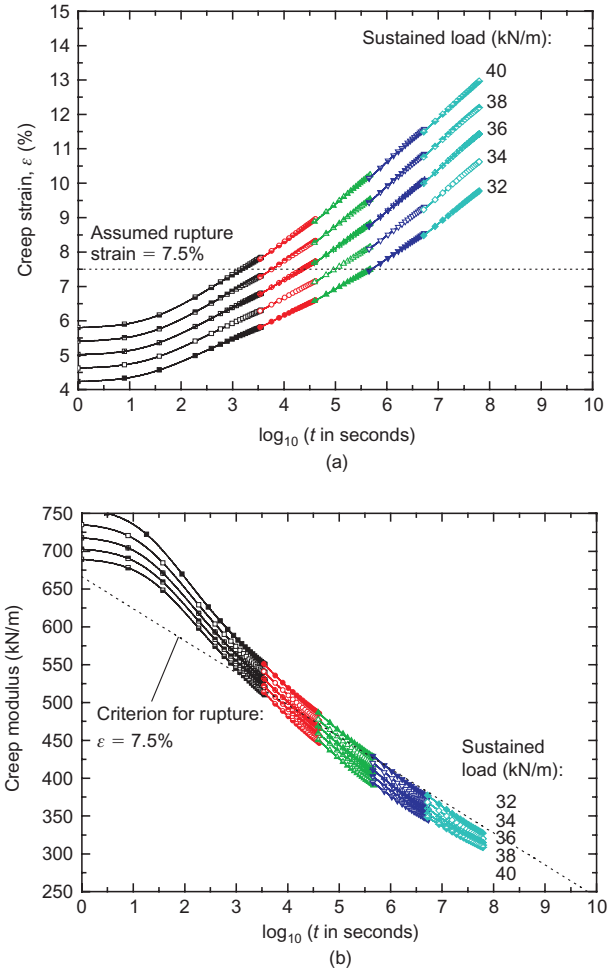

Figure 22. Master curves in terms of (a) creep strain and (b) creep modulus, obtained from numerical TTS tests

by numerical tests employing several specific assumptions, as described in the preceding sections. If the respective numerical tests are relevant, their results should be consistent with those obtained by experiments performed under otherwise the same conditions. Kongkitkul *et al.* (2007) performed a series of 30-day sustained loading tests on several types of polymer geosynthetic reinforcement with controlled initial creep strain rates, and showed that the overall tensile load–strain relations as well as the time histories of creep strain for 30 days from the experiment can be directly simulated by the procedures employed in the present study (i.e. the direct simulation). However, a set of sustained loading tests that lasted much longer than 30 days as well as TTS or SIM tests performed under otherwise the same test conditions as the long-term creep tests, all with controlled initial creep strain rates, cannot be found in the literature. Further study is necessary and required in this respect.

When the constitutive model based on the nonlinear three-component model (Figure 2) can be validated for a given type of polymer geosynthetic reinforcement, the master curves and creep rupture curves for the TTS and SIM test conditions can be constructed by the model simulation using parameters determined based on the results of a limited number of tests performed under limited test conditions. The important advantageous features of the constitutive model presented in this paper include the following.

- It becomes possible to predict not only the creep behaviour under TTS or SIM test conditions but also the tensile load–strain–time behaviour for arbitrary histories of tensile strain (or load), its rate and temperature.
- The model can be smoothly incorporated into an FEM code to analyse the deformation and stability of geosynthetic-reinforced soil structures subjected to arbitrary histories of load, its rate and temperature (e.g. Kongkitkul *et al.* 2004b; Tatsuoka *et al.* 2004; Noguchi *et al.* 2006; Siddiquee *et al.* 2006).

5. CONCLUSIONS

A non-linear three-component model was modified to describe the elasto-viscoplastic strength and deformation of polymer geosynthetic reinforcement subjected to arbitrary temperature changes. In this constitutive model, the negative effects associated with an increase in the ambient

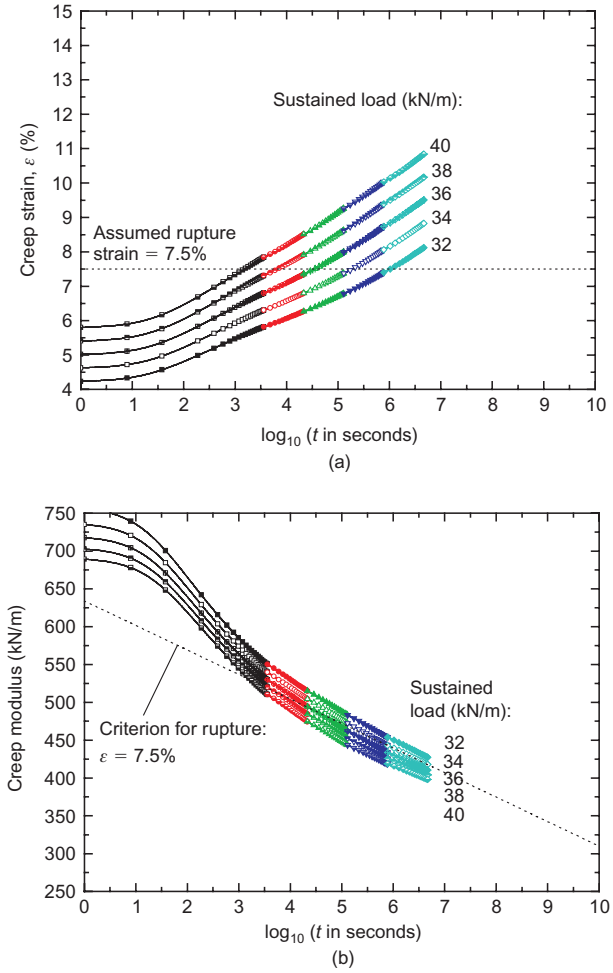

Figure 23. Master curves in terms of (a) creep strain and (b) creep modulus, obtained from numerical SIM tests

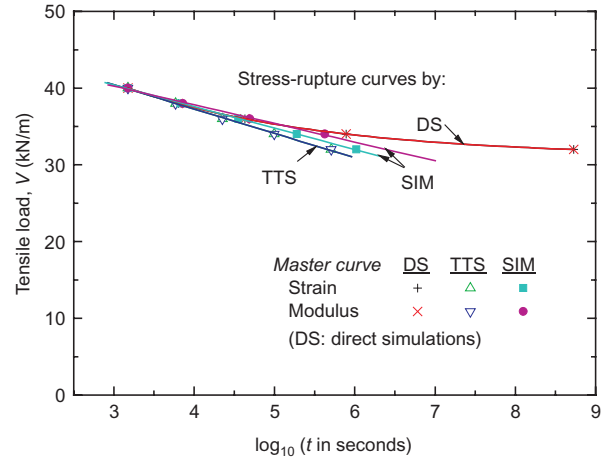

Figure 24. Creep–rupture curves obtained by the analysis of results from direct simulations and numerical TTS and SIM tests

temperature on the load–strain properties are taken into account in addition to the loading rate effects due to viscous properties. Therefore the model can be used to predict the load–strain behaviour of a given type of geosynthetic reinforcement when subjected to arbitrary histories of strain, strain rate and temperature.

The constitutive model was used to simulate the tensile load–strain–time behaviour including direct simulations of creep behaviour during 50-year sustained loading at a constant temperature and numerical simulations of load–strain–time behaviour at different elevated temperatures in TTS and SIM tests. It is shown that the proposed model can simulate the long-term SL as well as the TTS and SIM tests in a consistent manner. Master creep strain/modulus curves were constructed from the results of the numerical TTS and SIM tests and then compared with the creep strain/modulus–log(time) relations obtained from direct simulations of long-term SL tests. The creep rupture curves subsequently constructed from the results of the direct simulations and the numerical TTS and SIM tests were similar for relatively short creep rupture time. However, they became different as the creep rupture time increased, and the difference became larger with an increase in the creep rupture time. It is proposed that this difference is due to the different lowest strain rates encountered in the tests, and to some different empirical procedures involved in the numerical TTS and SIM tests. It is argued, based on the results of simulation described above, that it is possible that, for a given type of geosynthetic reinforcement, the TTS and SIM techniques underestimate the actual creep rupture strength after long times.

ACKNOWLEDGEMENTS

This study was supported by the Japan Society for the Promotion of Science through the grant ‘Advanced application of soil reinforcement technology to highly earthquake-resistant reinforcement of existing soil structures and construction of highly earthquake-resistant and environment-friendly soil structures’. The authors are also grateful to D. Hirakawa for his help, discussions and advice.

NOTATIONS

Basic SI units are given in parentheses.

A^f ageing function (dimensionless)
a^f parameter of the ageing-incorporated non-linear three-component model (dimensionless)
b parameter of viscosity function (dimensionless)
b^f parameter of the ageing-incorporated non-linear three-component model (dimensionless)
E^f yield inviscid tensile load increment that changes by irreversible strain increment (dimensionless)
E_0^f basic tangent stiffness that is independent of any ageing effects (N/m)
E_{eq} equivalent elastic stiffness (N/m)
F^f yield inviscid tensile load increment that changes by time increment (dimensionless)
g_v viscosity function of non-linear three-component model (dimensionless)
T ambient temperature (K)
t time used in the integration for a given step of loading and/or general time (s)

$\mathrm{d}t$ time increment used in the integration for a given step of loading (s)
t_c time with a fixed origin defined at the start of ageing (s)
t_{c1} time at the start of loading (s)
t' time that has elapsed until the start of sustained loading at an elevated temperature in numerical SIM tests (s)
Δt time increment during a process of temperature elevation (s)
V tensile load (N/m)
$\dot{V}$ tensile load rate (N/m s)
V^{f} inviscid tensile load of non-linear three-component model (N/m)
$\mathrm{d}V^{\mathrm{f}}$ inviscid tensile load increment used in the integration for a given step of loading (N/m)
$V^{\mathrm{f}}_{\mathrm{y}}$ yield inviscid load of non-linear three-component model (N/m)
$\mathrm{d}V^{\mathrm{f}}_{\mathrm{y}}$ yield inviscid tensile load increment used in the integration for a given step of loading (N/m)
V^{v} viscous tensile load of non-linear three-component model (N/m)
$V^{\mathrm{v}}_{\mathrm{iso}}$ viscous tensile load of isotach type (N/m)
V^{f}_0 basic inviscid load that is independent of any ageing effects (N/m)
α^* parameter of viscosity function (dimensionless)
α^{f} parameter of the ageing-incorporated non-linear three-component model (dimensionless)
ε tensile strain (dimensionless)
$\varepsilon^{\mathrm{ir}}_1$ irreversible strain at the start of loading (dimensionless)
$\mathrm{d}\varepsilon^{\mathrm{ir}}$ irreversible strain increment (dimensionless)
$\dot{\varepsilon}$ tensile strain rate (s^{-1})
$\dot{\varepsilon}^{\mathrm{e}}$ elastic strain rate (s^{-1})
$\dot{\varepsilon}^{\mathrm{ir}}$ irreversible strain rate (s^{-1})
$\dot{\varepsilon}^{\mathrm{ir}}_0$ parameter of viscosity function (s^{-1})
τ irreversible strain used in the integration for a given step of loading (dimensionless)
$\mathrm{d}\tau$ irreversible strain increment used in the integration for a given step of loading (dimensionless)

ABBREVIATIONS

ML monotonic loading
SL sustained loading
TTS time–temperature superposition
SIM stepped isothermal method

REFERENCES

ASTM D6992. *Standard Test Method for Accelerated Tensile Creep and Creep-rupture of Geosynthetic Materials Based on Time–temperature Superposition Using the Stepped Isothermal Method*. ASTM International, West Conshohocken, PA.

Allen, S. R. (2003). Considerations on the stepped isothermal method: a breather on the way of widespread use. *Proceedings of the GRI-17 Conference on Hot Topics in Geosynthetics*, Folson, PA, pp. 292–311.

Baras, L. C. S., Bueno, B. S. & Costa, C. M. L. (2002). On the evaluation of stepped isothermal method for characterizing creep properties of geotextiles. *Proceedings of the 7th International Conference on Geosynthetics*, Nice, France, Vol. 4, pp. 1515–1518.

Bueno, B. S., Costanzi, M. A. & Zornberg, J. G. (2005). Conventional and accelerated creep tests on nonwoven needle-punched geotextiles. *Geosynthetics International*, **12**, No. 6, 276–287.

Di Benedetto, H., Sauzéat, C. & Geoffroy, H. (1999). Modelling viscous effects for sand and behaviour in the small strain domain. *Proceedings of the 2nd International Symposium on Pre-failure Deformation Characteristics of Geomaterials*, IS Torino, Vol. 2, pp. 1357–1367.

Di Benedetto, H., Tatsuoka, F. & Ishihara, M. (2002). Time-dependent shear deformation characteristics of sand and their constitutive modelling. *Soils and Foundations*, **42**, No. 2, 1–22.

Di Benedetto, H., Tatsuoka, F., Lo Presti, D., Sauzéat, C. & Geoffroy, H. (2005). Time effects on the behaviour of geomaterials. *Deformation Characteristics of Geomaterials: Recent Investigations and Prospects* (Di Benedetto, H., Doanh, T., Geoffroy, H. & Sauzéat, C. (eds)). Balkema, Rotterdam, pp. 59–123.

Ferry, J. D. (1980). *Viscoelastic Properties of Polymers*, 3rd edn. Wiley, New York.

Greenwood, J. H., Kempton, G. T., Brady, K. C. & Watts, G. R. A. (2004). Comparison between stepped isothermal method and long-term creep tests on geosynthetics. *Proceedings of the 3rd European Geosynthetics Conference (EuroGeo 3)*, Munich, Vol. 2, pp. 527–532.

GRI (2000). *Standard Test Method for Accelerated Tensile Creep and Creep-rupture of Geosynthetic Materials Based on Time–temperature Superposition Using the Stepped Isothermal Method*. Geosynthetic Research Institute, Drexel University.

Hirakawa, D., Kongkitkul, W., Tatsuoka, F. & Uchimura, T. (2003). Time-dependent stress–strain behaviour due to viscous properties of geogrid reinforcement. *Geosynthetics International*, **10**, No. 6, 176–199.

Hsieh, C., Lee, I. & Tain, Y. (2006). Creep strains of high strength polyester geogrids measured by conventional and accelerated test methods. *Proceedings of the 8th International Conference on Geosynthetics,* Yokohama, Japan, Vol. 4, pp. 1581–1584.

Kongkitkul, W., Hirakawa, D., Tatsuoka, F. & Uchimura, T. (2004a). Viscous deformation of geosynthetic reinforcement under cyclic loading conditions and its model simulation. *Geosynthetics International*, **11**, No. 2, 73–99.

Kongkitkul, W., Siddiquee, M. S. A., Hirakawa, D. & Tatsuoka, F. (2004b). FEM simulation of viscous behaviour of geogrid and geogrid-reinforced sand. *Proceedings of the 19th Geosynthetics Symposium (Japan Chapter of IGS)*, Tokyo, pp. 237–244.

Kongkitkul, W., Hirakawa, D. & Tatsuoka, F. (2005). A constitutive model to simulate the load–strain–time behaviour of geotextile reinforcement in TTS and SIM tests. *Proceedings of the 20th Geosynthetics Symposium (Japan Chapter of IGS)*, Tokyo, pp. 263–270.

Kongkitkul, W., Hirakawa, D. & Tatsuoka, F. (2007). Viscous behaviour of geogrids; experiment and simulation. *Soils and Foundations*, **47**, No. 2.

Koo, H., Kim, D. & Kim, Y. (2006). The stepped isothermal method for lifetime prediction of PET geogrids sheathed in PP. *Proceedings of the 8th International Conference on Geosynthetics,* Yokohama, Japan, Vol. 4, pp. 1555–1558.

Narejo, D. & Allen, S. (2004). Using the stepped isothermal method for geonet creep evaluation. *Proceedings of the 3rd European Geosynthetics Conference (EuroGeo 3)*, Munich, Vol. 2, pp. 539–544.

Noguchi, T., Kongkitkul, W., Hirakawa, D. & Tatsuoka, F. (2006). FE analysis on the rate-dependent behaviour of model geosynthetic-reinforced soil retaining wall. *Proceedings of the 8th International Conference on Geosynthetics*, Yokohama, Japan, Vol. 4, pp. 1357–1360.

Shinoda, M. & Bathurst, R. J. (2004). Strain measurement of geogrids using a video-extensometer technique. *Geotechnical Testing Journal*, **27**, No. 5, 456–463.

Siddiquee, M. S. A., Tatsuoka, F. & Tanaka, T. (2006). FEM simulation of the viscous effects on the stress–strain behaviour of sand in

plane strain compression. *Soils and Foundations*, **46**, No. 1, 99–108.

Tatsuoka, F., Ishihara, M., Di Benedetto, H. & Kuwano, R. (2002). Time-dependent deformation characteristics of geomaterials and their simulation. *Soils and Foundations*, **42**, No. 2, 106–132.

Tatsuoka, F., Di Benedetto, H. & Nishi, T. (2003). A framework for modelling of the time effects on the stress–strain behaviour of geomaterials. *Proceedings of the 3rd International Symposium on Deformation Characteristics of Geomaterials, IS Lyon 2003*, Lyon, pp. 1135–1143.

Tatsuoka, F., Hirakawa, D., Shinoda, M., Kongkitkul, W. & Uchimura, T. (2004). An old but new issue: viscous properties of polymer geosynthetic reinforcement and geosynthetic-reinforced soil structures. Keynote lecture. *Proceedings of the 3rd Asian Regional Conference on Geosynthetics (GeoAsia 2004)*, Seoul, pp. 29–77.

Tatsuoka, F., Kongkitkul, W. & Hirakawa, D. (2006). Viscous property and time-dependent degradation of geosynthetic reinforcement. *Proceedings of the 8th International Conference on Geosynthetics*, Yokohama, Japan, Vol. 4, pp. 1587–1590.

Thornton, J. S., Paulson, J. N. & Sandri, D. (1998). Conventional and stepped isothermal methods for characterizing long term creep strength of polyester geogrids. *Proceedings of the 6th International Conference on Geosynthetics*, Atlanta, GA, pp. 691–698.

Thornton, J. S. & Baker, T. L. (2002). Comparison of SIM and conventional methods for determining creep-rupture behavior of a polypropylene geotextile. *Proceedings of the 7th International Conference on Geosynthetics*, Nice, France, Vol. 4, pp. 1545–1550.

Zornberg, J. G. & Kavazanjian, E. Jr (2002). Closures on: 'Prediction of the performance of a geogrid-reinforced slope founded on solid waste'. *Soils and Foundations*, **42**, No. 5, 129–130.

Zornberg, J. G., Byler, B. R. & Knudsen, J. W. (2004). Creep of geotextiles using time–temperature superposition methods. *Journal of Geotechnical and Geoenvironmental Engineering, ASCE*, **130**, No. 11, 1158–1168.

The Editors welcome discussion on all papers published in Geosynthetics International. Please email your contribution to discussion@geosynthetics-international.com by 15 August 2007.